Fusion Engineering and Design 216 (2025) 115080

Contents lists available at ScienceDirect

Fusion Engineering and Design

journal homepage: www.elsevier.com/locate/fusengdes

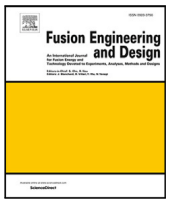

Enhancing computational efficiency in nuclear fusion through reduced order modelling: Applications in magnetohydrodynamics

Matteo Lo Verso [a], Stefano Riva [a], Carolina Introini [a], Eric Cervi [a], Luciana Barucca [b], Marco Caramello [b], Matteo Di Prinzio [b], Francesca Giacobbo [a], Laura Savoldi [c], Antonio Cammi [d,a,*]

[a] Energy Department - Nuclear Reactors Group, Politecnico di Milano, Via La Masa 34 Milan, 20156, Italy
[b] Ansaldo Nucleare SpA, Genova, Italy
[c] MATHEP Group, Dept. of Energy "Galileo Ferraris", Politecnico di Torino, Torino, Italy
[d] Emirates Nuclear Technology Center, Department of Mechanical and Nuclear Engineering, Khalifa University, Abu Dhabi, 127788, United Arab Emirates

ARTICLE INFO

Keywords:
Magnetohydrodynamics
Magnetic confinement fusion
Fusion reactors
Reduced order modelling
Dynamic Mode Decomposition

ABSTRACT

Magnetohydrodynamics (MHD) studies the dynamics of electrically conducting fluids under the influence of a magnetic field and it is relevant in several nuclear applications. However, the high computational cost of multi-physics MHD simulations poses a challenge. Reduced Order Modelling (ROM) offers a promising alternative, enabling lower-dimensional approximations while preserving accuracy. This allows for a reduction in the computational time and, at the same time, accurate approximations of the intricate physics involved in fusion reactors. However, ROM techniques are relatively new within the MHD framework, and benchmark test cases should be considered in this first stage for verification and validation. Therefore, this study applies the ROM methodology to a MHD scenario to study their potentialities (and eventual criticalities) for this class of problems. The benchmark test case considered in this work is the Backward-Facing Step. The obtained results contribute to assessing the capabilities of ROM methodologies in MHD scenarios, demonstrating their potential to enhance computational efficiency in this field and representing a critical step towards advancing the computational modelling of complex systems in nuclear fusion.

1. Introduction

Magnetohydrodynamics (MHD) investigates the dynamics of electrically conductive fluids, specifically those with significant electrical conductivity, flowing in the presence of a magnetic field [1]. This theory provides mathematical models which are extensively applied in nuclear research. In particular, this theory is exploited in magnetic confinement fusion (MCF) mainly for describing thermonuclear plasmas, which can be treated as conducting fluids confined by high-intensity magnetic fields [2]. Moreover, MHD models may also be employed for the description of conductive fluids foreseen in the design of many tokamaks blankets, like liquid metals [3] or molten salts [4]. In tokamaks, magnetic fields are used to confine the plasma within the vacuum vessel; at the same time, residual magnetic fields may interact with conductive fluids operating in the blanket, influencing their fluid dynamics. Then, the blanket design must consider the influence of magnetic fields varying in magnitude and direction over time, which could potentially modify the flow regime of the fluids inside. Beyond fusion reactor applications, MHD theory may be exploited for the analysis of innovative engineering systems employing conducting fluids subjected to an electromagnetic field, as the magnetic field could improve the thermal-hydraulics and overall dynamics of the operating fluid, including pressure drops, velocity, thermal diffusion, and flow regime. It is then imperative to clearly understand the specific effects of the magnetic field on the dynamics of these fluids.

The detailed description of MHD problems requires a multi-physics framework, as fluid velocity and magnetic field are coupled; thus, a non-linear system of coupled partial derivative equations needs to be solved [5]. Due to the complex interactions between the various physics at play, high-fidelity numerical investigations represent the current state-of-the-art for exploring MHD phenomena: the specific MHD effects strongly depend on the shape and intensity of the applied magnetic field and oscillations in the magnetic profile can substantially perturb the stability of the system [6]. However, accounting for all the possible combinations of parameters (magnetic field intensity, direction, inlet velocity...) is computationally unfeasible when using high-fidelity models; additionally, the use of high-fidelity models becomes unpractical

* Corresponding author.
E-mail address: antonio.cammi@polimi.it (A. Cammi).

https://doi.org/10.1016/j.fusengdes.2025.115080
Received 19 December 2024; Received in revised form 19 March 2025; Accepted 10 April 2025
Available online 26 April 2025

for real-time applications, including online control. On one hand, they are able to forecast the future state of the system with great accuracy; on the other hand, their computational times are such that any real-time action becomes unfeasible. For this reason, it is particularly important to find strategies to reduce the computational complexity characteristic of MHD simulations.

In this framework, Reduced Order Modelling (ROM) techniques [7,8] represent a promising solution for minimizing the computational burden by approximating complex systems with surrogate models, especially in real-time scenarios, where multiple evaluations of the high-fidelity model must be performed [9]. These methodologies can reduce computational costs while maintaining accuracy at an acceptable levels. Specifically, they are often adopted to simulate unexplored fluid dynamics scenarios [10–13], multi-physics scenarios [14,15] and sensitivity analyses, without solving the original equations. In practice, the ROM approach could allow to derive a general reduced model able to quickly reconstruct a MHD scenario for any value of a considered parameter, such as for example the magnetic profile. Moreover, the speed-up of numerical computations would allow the application of ROM techniques in real-time contexts, such as control-oriented applications, where it is crucial to rapidly assess the instantaneous effects of residual magnetic fields on the blanket fluids for operational and safety reasons.

The logic underlying ROM methodologies is the following. The ROM approach aims at finding a reduced representation of the original full-order model (FOM), starting from some training solutions (called snapshots), which accurately describe the physical problem. From these snapshots, the ROM technique retrieves a set of spatial basis functions, which embeds the spatial dependency and which spans a reduced space which well represents the high-dimensional one. The latent temporal dynamics are then computed within this reduced space, obtaining a reduced model with much lower dimensionality than the high-fidelity one. Then, the obtained reduction is effectively helpful if the computational cost to obtain an approximation of the solution for an unseen parameter using the reduced model is short compared to that of the FOM, whilst keeping the desired accuracy. In the field of magnetohydrodynamics, the application of ROM techniques is still in its infant stages, especially for what concerns conductive liquid metals. Conversely, literature regarding applications for thermonuclear plasmas is wider. Taylor et al. [16] adopted the Dynamic Mode Decomposition (DMD) for the diagnostic analysis of the non-linear dynamics of a magnetized plasma in resistive MHD; Kaptanoglu et al. [17] applied a data-driven version of the Proper Orthogonal Decomposition (POD) Galerkin models for compressible plasmas, relying on physically constrained sparse-identification of non-linear dynamics [18]; moreover Kaptanoglu et al. [19] exploited DMD to extract spatio-temporal magnetic coherent structures from the experimental and numerical datasets of the HIT-SI (Helicity Injected Torus with Steady Inductive Helicity Injection) experiment. Regarding instead conductive fluids (such as those foreseen for the tokamak blankets), there are very few studies in the literature. The authors proposed in a previous paper a non-intrusive POD combined with Gaussian Process Regression for the MHD flow of a liquid metal over a Backward Facing Step (BFS) geometry [20]. That study demonstrated the suitability of the ROM methodology to generate simplified models that can accurately represent the MHD effects exerted by residual magnetic fields of any intensity on operating fluids flowing within the blanket, starting from training solutions for specific values of the magnetic field.

This work builds from the results of [20] and aims at further studying the potentialities of the Reduced Order Modelling approach for predicting the temporal evolution of MHD scenarios given a certain dataset truncated in time. For this purpose, the Dynamic Mode Decomposition is applied to analyse the dynamics of magnetohydrodynamic flows of lead-lithium in a Backward Facing Step (BFS) and to forecast the evolution of the flow regime, focusing on the creation of surrogate models containing adequate information from the high-fidelity data such that they can accurately retrieve the latent temporal dynamics. The procedure adopted aims at finding a reduced representation of the training snaphosts, which consists of a time series dataset, obtained numerically solving the full-order model associated to the considered magnetohydrodynamic scenario. The structure of the present paper is now reported. Section 2 provides an overview of the reduced order modelling approach, emphasizing the specific technique adopted in this work. Section 3 describes the MHD model and presents the numerical results obtained with the DMD approach. Finally, Section 4 resumes the main conclusions of the present work.

2. Dynamic mode decomposition

Dynamic Mode Decomposition (DMD) is a technique developed by Schmid in [21] to identify spatial and temporal coherent structures from high-dimensional data for fluid dynamics applications. Briefly, this algorithm is based on the Singular Value Decomposition (SVD) [22]. Given a matrix $\mathbb{X} \in \mathbb{R}^{\mathcal{N}_h \times N_t}$, its low M-rank representation reads,[1] as Eq. (1)

$$\mathbb{U}_M \, \Sigma_M \, \mathbb{V}_M^* \approx \mathbb{X} \tag{1}$$

in which $\mathbb{U}_M \in \mathbb{R}^{\mathcal{N}_h \times M}$ is an orthogonal matrix containing the left singular vectors, also called spatial modes, $\Sigma_M \in \mathbb{R}^{M \times M}$ is a diagonal matrix containing the singular values, measuring the importance of each mode, $\mathbb{V}_M^* \in \mathbb{R}^{M \times N_t}$ is an orthogonal matrix with the right singular vectors [9].

The DMD algorithm provides a modal decomposition where each mode consists of spatially correlated structures that have the same linear behaviour in time (e.g., oscillations at a given frequency with growth or decay), thus finding the linear coordinate system that best fits the starting data. By ranking the modes through the singular values of the starting data matrix, DMD builds a low-dimensional surrogate linear model that can simulate the temporal evolution of these spatial modes.

This work adopts the implementation of the DMD within the *pyDMD* package [23,24], whose implementation is briefly outlined below. The DMD algorithm is inherently data-driven: the first step consists in collecting time-series snapshots of the high-fidelity state vector $\mathbf{x}(t_k) \in \mathbb{R}^{\mathcal{N}_h}$, with $\mathcal{N}_h$ being the dimension of the state vector, at different time steps uniformly sampled [21,22]. In particular, the resulting snapshot matrix must be shaped as in Eq. (2)

$$\mathbb{X} = [\mathbf{x}(t_1) \mid \mathbf{x}(t_2) \mid \cdots \mid \mathbf{x}(t_{N_t})] \in \mathbb{R}^{N_h \times N_t} \tag{2}$$

The DMD seeks the best-fit linear operator $\mathbb{A}$ that allows the system to advance in time, as in Eq. (3)

$$\mathbf{x}_{k+1} \approx \mathbb{A}\mathbf{x}_k \tag{3}$$

given $\mathbf{x}_k = \mathbf{x}(t_k)$. The operator $\mathbb{A}$ describes the dynamics of the associated **linear** system that best advances the snapshots forward in time. Mathematically, this operator is the solution of the minimization problem

$$\mathbb{A} = \underset{\mathbb{A}^\star \in \mathbb{R}^{\mathcal{N}_h \times \mathcal{N}_h}}{\arg\min} \; \|\mathbb{X}^+ - \mathbb{A}^\star \mathbb{X}^-\|_F = \mathbb{X}^+ (\mathbb{X}^-)^\dagger \tag{4}$$

given the snapshots matrices $\mathbb{X}^- = [\mathbf{x}(t_1) \mid \cdots \mid \mathbf{x}(t_{N_t-1})] \in \mathbb{R}^{N_h \times (N_t-1)}$ and $\mathbb{X}^+ = [\mathbf{x}(t_2) \mid \cdots \mid \mathbf{x}(t_{N_t})] \in \mathbb{R}^{N_h \times (N_t-1)}$, $\|\cdot\|_F$ being the Frobenius norm and the superscript † indicating the pseudo-inverse [22]. This optimization version of the DMD algorithm generalizes the exact DMD proposed by [21] to perform a regression to exponential-time dynamics, thus providing an improved computation of the DMD modes and their eigenvalues [25].

However, for very high dimensional data, like the one coming from fluid dynamics simulations, the number of elements of $\mathbb{A}$ may

[1] The conjugate transpose of a matrix is indicated with superscript *.

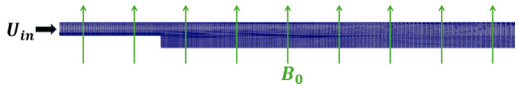

Fig. 1. Backward-facing step benchmark geometry.

be too high to be computed; therefore, it is convenient to represent this operator with a reduced coordinate system. The DMD algorithm leverages dimensionality reduction to evaluate the dominant eigenvalues and eigenvectors of the best-fit linear operator and to avoid the computation of the pseudo-inverse $(\mathbb{X}^-)^\dagger$. Tu et al. [26] proved the strong connection between the reduced eigenvalues and the true ones of $\mathbb{A}$. The dimensionality reduction is performed exploiting the Singular Value Decomposition [22]; the overall procedure is reported in Appendix.

Typically, the advancement in time (both to perform testing and forecasting) is performed following the spectral decomposition of $\tilde{\mathbb{A}}$, i.e.

$$\tilde{\mathbb{A}}\mathbb{W} = \mathbb{W}\Lambda \tag{5}$$

with $\mathbb{W}$ being the eigenvectors matrix and the diagonal matrix Λ containing the associated eigenvalues, which corresponds to the ones of $\mathbb{A}$ [26], embedding the dynamical evolution of the system. The former are needed to compute the so-called high-dimensional DMD modes $\boldsymbol{\Phi}$, i.e.

$$\boldsymbol{\Phi} = \mathbb{X}^+\mathbb{V}_M\,\Sigma_M^{-1}\mathbb{W} \tag{6}$$

which can be proved to be the eigenvectors of $\mathbb{A}$ [26].

All the previous operations are to be performed during the offline/train phase, whereas during the online/test the solution can be reconstructed for unknown time values. Especially, the above spectral decomposition allows for a quite simple expression for the advancement in time through the expansion

$$\mathbf{x}_k \approx \sum_{j=1}^{M} \phi_j \lambda_j^{k-1} b_j \tag{7}$$

given $\boldsymbol{\phi}_j \in \mathbb{R}^{\mathcal{N}_h}$ the jth column of $\boldsymbol{\Phi}$, λ_j the jth diagonal element of Λ and b_j the mode amplitude computed from the projection of the initial condition onto the reduced space, i.e. $\mathbf{b} = \boldsymbol{\Phi}^*\mathbf{x}_1$. The advancement in time of the solution occurs in the reduced space. Subsequently, through a decoding procedure, the solution is reprojected into the original space to provide a physically meaningful representation.

3. Numerical results

The two-dimensional Backward-Facing Step (BFS) is a well-known numerical benchmark for Computational Fluid Dynamics. This geometry has been selected for the present study, considering as a conducting fluid lead-lithium. The geometry and numerical mesh are shown in Fig. 1. In this work, as explained in Section 2, the DMD technique is adopted for forecasting the temporal evolution of the system.

The flow is initially stagnant, and a perpendicular magnetic field is imposed at time $t = 0$. Walls are considered no-slip and perfectly conducting; at the inlet, a uniform velocity is imposed, whereas at the outlet an external pressure condition is assumed. The magnetohydrodynamic model [27] that describes the incompressible, viscoresistive lead-lithium flow subjected to the setup outlined above is:

$$\begin{cases}
\nabla\cdot\mathbf{u} = 0 & \text{in } V,\ t>0\\
\rho\frac{\partial\mathbf{u}}{\partial t} + \rho(\mathbf{u}\cdot\nabla)\mathbf{u} = -\nabla p + \mu\Delta\mathbf{u} + \left(\frac{1}{\mu_0}\nabla\times\mathbf{B}\right)\times\mathbf{B} & \text{in } V,\ t>0\\
\frac{\partial\mathbf{B}}{\partial t} = \nabla\times(\mathbf{u}\times\mathbf{B}) + \frac{\eta}{\mu_0}\Delta\mathbf{B} & \text{in } V,\ t>0\\
\nabla\cdot\mathbf{B} = 0 & \text{in } V,\ t>0\\
\mathbf{u} = \mathbf{0} & \text{in } V,\ t=0\\
\mathbf{B} = \mathbf{B}_0 & \text{in } V,\ t=0\\
\mathbf{u} = \mathbf{u}_{in} & \text{on } \Gamma_{inlet},\ t>0\\
\frac{\partial\mathbf{u}}{\partial\mathbf{n}} = 0 & \text{on } \Gamma_{outlet},\ t>0\\
\mathbf{u} = \mathbf{0} & \text{on } \Gamma_{walls},\ t>0\\
\frac{\partial\mathbf{B}}{\partial\mathbf{n}} = 0 & \text{on } \partial V,\ t>0\\
p = p_{ext} & \text{on } \Gamma_{outlet},\ t>0\\
\frac{\partial p}{\partial\mathbf{n}} = 0 & \text{on } \partial V\backslash\Gamma_{outlet},\ t>0
\end{cases} \tag{8}$$

where V denotes the domain, ∂V the entire boundary, Γ are the surfaces of the boundary and t is the time. Moreover, $\mathbf{u}$ represents the fluid velocity, p the pressure, $\mathbf{B}$ the magnetic field, ρ the density, μ the dynamic viscosity, μ_0 the magnetic permeability and η the electrical resistivity. For a full description of the selected mesh numerical parameters and lead-lithium thermo-physical values refer to [20].

The introduced model is the full-order model (FOM), representing the considered MHD scenario. This model was used to generate the training snapshots in OpenFOAM, exploiting the custom-made MHD solver **magnetoHDFoam** developed by the authors and presented in [28]. This library implements a magnetic version of the well-known PIMPLE algorithm, in which the magnetic component has been included. The solver is available on Github under the MIT license.

3.1. Offline phase

In the offline phase, the FOM is solved directly to create the training high-fidelity snapshots for velocity $\mathbf{u}$ and pressure $\tilde{p}$.[2] The time range is 2 s, with a uniform sampling time of 0.02 s. From this dataset, a training set Ξ^{test} was extracted that includes only a portion of the snapshots (from 0 to 1.44 s, i.e. 72% of snapshots data), while the remaining data formed the test set Ξ^{test}. This subdivision follows a standard approach for data-driven methods to have roughly three-fourth of the data for training and the remaining for testing: the surrogate model is trained with only a part of the available data, while the accuracy of the model will be evaluated by comparing the approximation of the reduced model with the data contained in the test set (that is, those unseen by the surrogate model).

At this stage, a preliminary SVD was applied to the training set to assess the decay of the singular values and the relative importance of the corresponding modes related to the training matrix. Indeed, through the SVD procedure the modes and associated singular values are ranked based on their information content (i.e., how much they are representative of the training high-fidelity dataset), in descending order [7–9].

In Fig. 2, both the behaviour of the singular values and the relative information/energy content as a function of the rank are illustrated. The singular values are indicated as σ_r (where r denotes the rank) while the relative information content is defined as

$$I(r) = 1 - \frac{\sum_{i=1}^{r}\sigma_i^2}{\sum_k \sigma_k^2}. \tag{9}$$

The singular values exhibit exponential decay for both the velocity and the reduced pressure. This implies that both quantities of interest can be approximated by a linear reduced subspace obtained from the dominant modes [29]. Moreover, the decay of the information/energy

[2] The pressure has been rescaled to the external pressure imposed at the outlet, i.e. $\tilde{p} = p - p|_{ext}$.

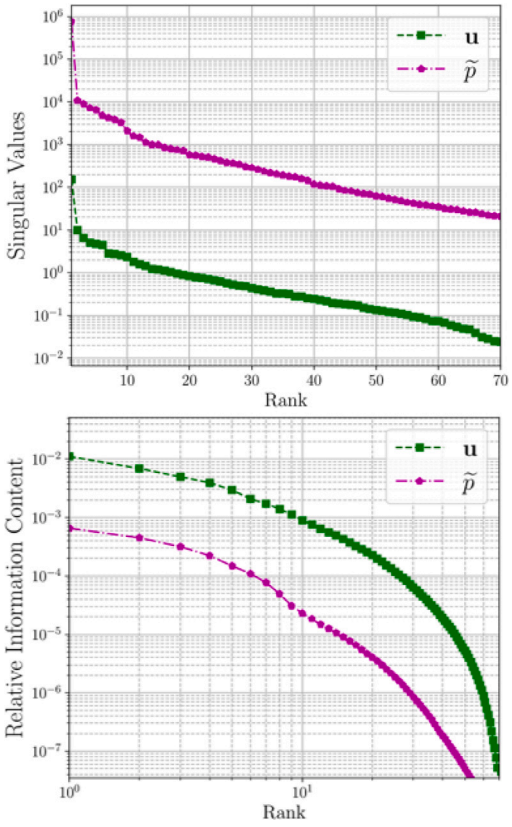

Fig. 2. SVD singular values (top) and information/energy content (bottom) as a function of the rank for the pressure and the velocity.

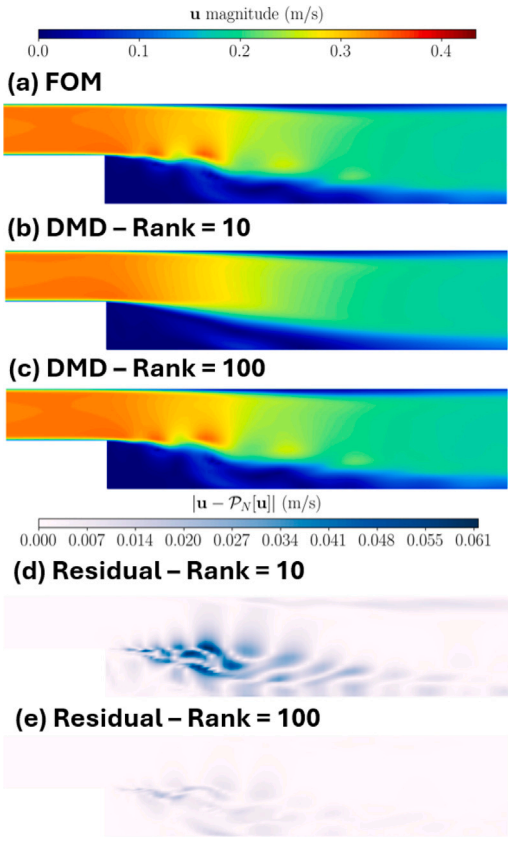

Fig. 3. Comparison between the FOM velocity magnitude and the DMD reconstruction, using 10 and 100 modes, with the associated residual field at $t = 1.92$ s. The figure is zoomed in on the step region.

content $I(r)$ shows how the error of low-rank falls below 10^{-3} for a rank equal to 10, signifying that the relative information content for this value is pretty good for both physical quantities. Thus, following the algorithm explained in Section 2, a reduced matrix $\tilde{\mathbb{A}}$ was generated from the training data, associated with the surrogate DMD model.

3.2. Online phase

In the following the results obtained during the online phase are presented, using the DMD model generated during the offline phase with a dimensionality equal to 10. For both the quantities of interest, the Dynamic Mode Decomposition was applied following the algorithm exposed in Section 2, with the aim to capture information regarding the most dominant physics. Finally, the temporal evolution of velocity and pressure fields was calculated by exploiting the DMD modes, using the temporal expansion shown in Eq. (7). In particular, the solution of the reduced model was advanced in time from 0 to 2 seconds, thus even for time instances not included in the training set Ξ^{train} with the aim of predicting the flow dynamics. At this point, the flow reconstructed with the reduced model was compared with the real solution, represented by the test set Ξ^{test}.

Figs. 3 and 4 show the velocity magnitude and pressure fields from the FOM test set (3a and 4a) and the DMD reconstruction using 10 modes (3b and 4b), considering a time instant outside the training set.

The dominant dynamics are captured well by the surrogate model; however, the smaller scales, corresponding to the small vortices after the step, have been filtered out by the DMD approximation, as already seen in [20]. Indeed, the reported residuals (Figs. 3d and 4d), defined as the difference between the exact and the approximated solutions, exhibit oscillations localized in the step region, where small-scale turbulence with faster dynamics than the DMD modes occurs. These may be captured either by increasing the sampling frequency or by increasing the dimensionality of the DMD model, thereby enhancing the accuracy of the reconstruction obtained from the DMD.

Nonetheless, the residual is sufficiently little for both the fields. Indeed, the residual is mostly localized after the step, resulting in very low spatial average values (0.003 m/s for the velocity and 7 Pa for the pressure), while the maximum values are 0.062 m/s for the velocity and 157 Pa for the pressure.

Moreover, the relative L^2-error related to the DMD reconstruction has been calculated for the two quantities of interest as

$$\epsilon_{\mathbf{u}} = \frac{\|\mathbf{u} - \mathcal{P}_N[\mathbf{u}]\|}{\|\mathbf{u}\|}, \quad \epsilon_{\widetilde{p}} = \frac{\|\widetilde{\mathbf{p}} - \mathcal{P}_N[\widetilde{\mathbf{p}}]\|}{\|\widetilde{\mathbf{p}}\|} \tag{10}$$

where $\|\cdot\|$ represents the classical L^2-norm. Fig. 5 shows the computed errors for the velocity and the pressure when a rank equal to 10 is selected.

The errors are relatively low and acceptable for both velocity and pressure. As already observed, they show significant oscillations at shorter times, which are attributed to the faster dynamics of the flow at those time scales, which have a frequency higher than the cut-off frequency of the DMD. However, both the maximum values (0.104 for the velocity and 0.027 for the pressure) and the averages over time (0.059 for the velocity and 0.016 for the pressure) of the errors are quite low for both the quantities. So, the generated DMD model reconstructs the dominant dynamics of the flow with an acceptable accuracy.

To try to capture even the faster dynamics corresponding to the recirculations after the step the same procedure was repeated with an increased value for the rank r. Figs. 3c and 4c represent the velocity and pressure field reconstructed imposing the rank of the reduced model

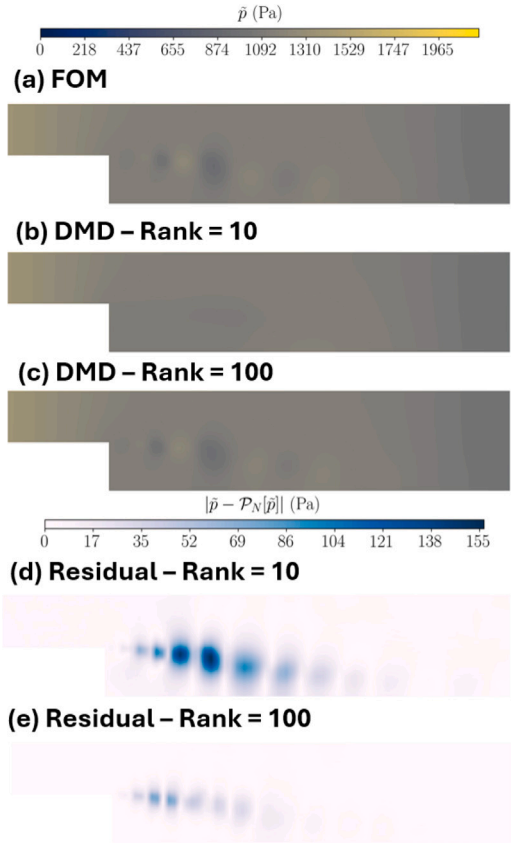

Fig. 4. Comparison between the FOM pressure and the DMD reconstruction, using 10 and 100 modes, with the associated residual field at $t = 1.92$ s. The figure is zoomed in on the step region.

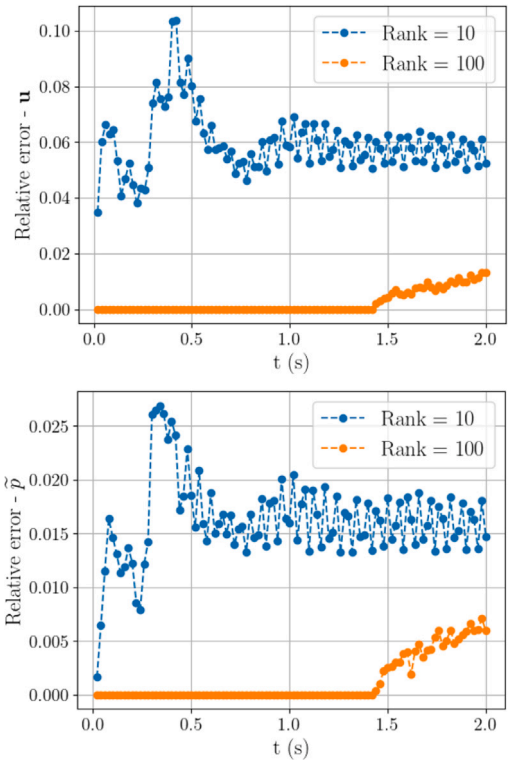

Fig. 5. Relative error over time for velocity (top) and pressure (bottom), using 10 modes and 100 modes. The circles represent the time sampling instants.

equal to 100, compared with the previous reconstruction operated with 10 basis (see Figs. 3b and 4b). Even with this rank, the reduced model has a significantly smaller size than the full-order matrix, which was composed of 7500 spatial points and 100 time instants.

From the figures, it is evident that the DMD benefits from the increase in rank in terms of accuracy. In fact, this second surrogate model, unlike the previous one, is able to capture even the small recirculation dynamics that occur near the step. This is due to the fact that such dynamics have high temporal frequencies, which were cut off by the previous more approximate model. Moreover, the residuals are lower for both the fields with average values of 0.0008 m/s and 1.88 Pa and maximum values of 0.21 m/s and 77 Pa respectively.

Successively, the relative error was computed in order to quantify the accuracy of the second model. Fig. 5 shows the relative error over time for the velocity magnitude and the pressure field for the DMD model with 100 basis. It is clear that the error in this second case is much lower compared to the error of the previous model. In particular, the error is almost negligible for the time instants contained in the training set, meaning that the reduced model with rank equal to 100 is able to almost perfectly reconstruct the dynamics of the full-order model that were used during the training phase. At subsequent times outside of the training set, the error obviously increases slightly but remains very small, lower than the error of the surrogate model with dimension 10.

Moreover, for the velocity field, an analysis was also conducted on the reconstruction of its two distinct components. Fig. 6 presents a comparison between the FOM solution and the DMD reconstruction, using 10 and 100 modes, for both the horizontal and vertical velocities. It can be observed that a sufficient number of bases allows for a highly accurate reconstruction of the individual velocity components. In fact, while the reconstruction with 10 modes shows notable differences, the DMD with 100 modes is able to reconstruct both velocity components with negligible residuals.

An analysis of the computational costs required by the resolution of the full-order model and the reconstruction performed by the DMD is now presented. The FOM simulation has been performed on an HPC cluster, whereas the DMD algorithm has been executed on a tower computer with an Intel Core i7-9800X processor. The resolution of the FOM required 1240 s, while the online phase of the two considered reduced models with 10 and 100 modes took 0.03 s and 0.04 s respectively. Thus, an increase in rank of one order of magnitude does not correspond to a similar increase in the computational time, skewing the trade-off between accuracy and computational times towards the former.

The benefit in terms of computational time is enormous when adopting the DMD approach, since the computational time is reduced by over 4 orders of magnitude. However, the increase in the reduced model rank results in an increase in computational burden, but in any case, compared to the time required by the full-order model, the difference between the computational costs of the two reduced models is very small. So, if the aim of the work is to reproduce the dominant average flow, a DMD model of even very small size can be considered. On the other hand, when also the physics at small time scales have to be taken into account, it is necessary to increase the dimensionality of the reduced model, slightly increasing the computational cost. In any case, regardless of the rank value selected for the reduced matrix, the computational times are drastically lower compared to the resolution of the full-order model.

Subsequently, the same technique was used considering different values of magnetic intensity, to examine if the approach is generalizable to any value of magnetic field. Different snapshots were generated, reproducing the same benchmark but subjected to different values of magnetic intensity, in particular $B_0 \in [0.1, 1.0]$ T, and the same DMD procedure was applied case by case, with 10 and 100 modes. The average relative L^2-error has been computed for each analysed case and the results are reported in Fig. 7.

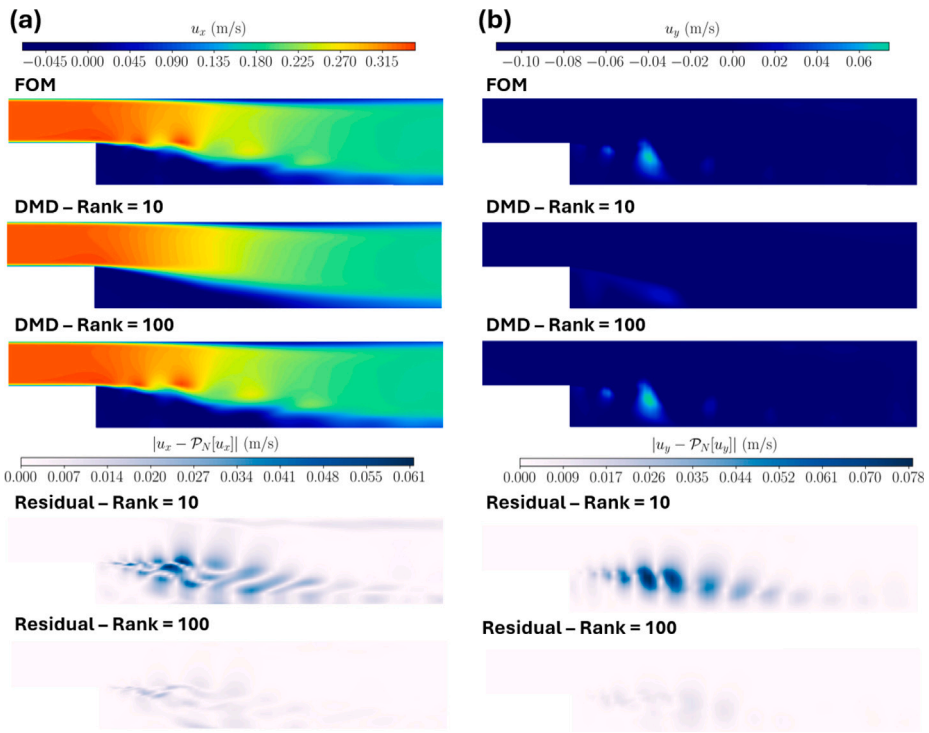

Fig. 6. Comparison between the FOM horizontal (a) and vertical (b) velocity components and the DMD reconstruction, using 10 and 100 modes, with the associated residual field at $t = 1.92$ s. The figure is zoomed in on the step region.

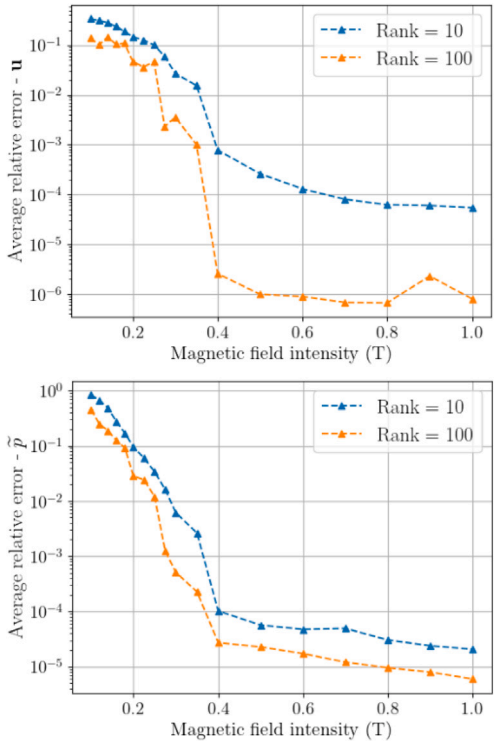

Fig. 7. Average relative error for velocity (top) and pressure (bottom) in logarithmic scale for different values of imposed magnetic field intensities, exploiting 10 and 100 modes.

It can be observed that in general the error is higher for very low magnetic fields, while for higher intensities it becomes smaller and smaller, for both the selected ranks. This is because the magnetic field tends to suppress turbulent dynamics and laminarize the flow [30]. Indeed, for very low magnetic fields, substantial recirculations in the step survive, and therefore there are high-frequency dynamics which are not completely captured. In these circumstances, increasing the number of modes allows only partially to reduce the relative error. This result shows that for low magnetic intensities, the selected number of temporal snapshots is not sufficient for capturing all the phenomena occurring at the smallest scales and a finer temporal sampling should be necessary for a more accurate reconstruction of the complicated turbulent dynamics. Conversely, for high enough magnetic field intensities, the accuracy improves significantly and an elevated number of modes permits to reduce drastically the relative error, in particular for the reconstruction of the velocity. This is related to the fact that, for intense enough magnetic fields, the flow is completely laminarized and all the dynamics at play are encompassed in the reduced model, especially if a reasonably large rank is selected. Finally, for even higher magnetic intensities, the relative error becomes negligible even for a small rank, meaning that even few modes are sufficient to encode the flow dynamics. These results highlight that both the generation of the snapshots and the dimensionality selection of the reduced model during the offline phase must be done with criterion based on physical considerations, so that the DMD model can be fully representative of the full-order model.

4. Conclusions

The present work applies a Dynamic Mode Decomposition approach to a magnetohydrodynamic scenario, consisting of lead-lithium flowing in a BFS geometry. The purpose of this work was to create a reduced model of very lower-dimension with respect to the full-order model, yet still sufficiently accurate, and that could also be able to do forecasting of time series. According to the authors' knowledge, this study represents one of the few works focusing on ROM for MHD flows involving fluids representing liquid metals flowing in breeding blankets, with the objective of creating accurate surrogate models capable of forecasting and extrapolation to unseen scenarios.

In the offline phase, the snapshots for the velocity and the pressure fields were generated solving the full-order model and a train set

had been extracted as subset of the entire dataset. Then, a reduced model has been produced, applying the DMD technique. During the online phase, the temporal evolution of velocity and pressure was reconstructed using the DMD model, even for time instants not included in the training snapshots. The obtained results were compared with the data belonging to the test set. The DMD model was able to reconstruct the unseen temporal behaviour of flow dynamics with an acceptable accuracy, with much lower computational costs compared to a full-order solution. In particular, the accuracy of DMD strongly depends on the dimension of the matrix associated to the reduced model, especially for catching the physics occurring at small time scales. Indeed, if the exploited snapshots are sufficiently dense to contain most of the information the flow dynamics, a sensitivity analysis on the dimensionality of the reduced model can allow, in principle, to build a reduced model able to reconstruct even the more intricate and chaotic phenomena related to turbulent dynamics, while keeping the computational burden very low. This study demonstrates the feasibility of reduction techniques to create surrogate models able to capture the MHD effects of residual magnetic fields on operational fluids within the blanket. Moreover, since DMD is a purely data-driven technique, similarly good results can be expected, in principle, for different configurations, eventually considering alternative initial or boundary conditions, provided that data are of sufficient quality. Thus, if the exploited snapshots fully represent the phenomenon under study, the approach may be extended to large-scale configurations, such as three-dimensional flows in the blanket or even MHD thermonuclear plasmas. So, the development of these models in nuclear fusion could greatly facilitate sensitivity analysis and uncertainty quantification by doing calculations at a reduced order level instead of a high-fidelity one. Moreover, the DMD approach, and more generally the ROM techniques, could enhance real-time simulations, which would be crucial in scenarios where controlling the effects of the magnetic field is imperative.

Future research could explore variants of the DMD approach in MHD scenarios, like the parametric version of the DMD, which, starting from different time series with different values of the magnetic field, generates a reduced model that generalizes the temporal evolution for any magnetic field intensity. Furthermore, these strategies may be explored in configurations involving more complex magnetic profiles, with arbitrary directions and orientations, as well as time-dependent conditions. Moreover, experimental data from measurement could be used as additional training data, thus augmenting the precision of the reduced model. Finally, it is foreseen to explore the potentialities of these methods in contexts involving realistic configurations that resemble actual scenarios found in fusion reactors, considering real geometries and more complex physics, taking into account also all the thermal effects including the energy equation.

CRediT authorship contribution statement

Matteo Lo Verso: Writing – original draft, Software, Methodology, Conceptualization. **Stefano Riva:** Writing – original draft, Software, Methodology, Conceptualization. **Carolina Introini:** Writing – review & editing. **Eric Cervi:** Writing – review & editing. **Luciana Barucca:** Writing – review & editing. **Marco Caramello:** Writing – review & editing. **Matteo Di Prinzio:** Writing – review & editing. **Francesca Giacobbo:** Writing – review & editing. **Laura Savoldi:** Writing – review & editing. **Antonio Cammi:** Writing – review & editing, Methodology, Conceptualization.

Declaration of competing interest

The authors declare that they have no known competing financial interests or personal relationships that could have appeared to influence the work reported in this paper.

Algorithm 1: Dynamic Mode Decomposition: operator learning

Input: Snapshot Matrix $\mathbb{X} = [\mathbf{x}(t_1) \mid \mathbf{x}(t_2) \mid \cdots \mid \mathbf{x}(t_{N_t})] \in \mathbb{R}^{N_h \times N_t}$
Output: Best fit operators $\mathbf{A}$ and $\tilde{\mathbf{A}}$

Generate time advancement matrices:
$\mathbb{X}^- = [\mathbf{x}(t_1) \mid \cdots \mid \mathbf{x}(t_{N_t-1})] \in \mathbb{R}^{N_h \times (N_t-1)}$;
$\mathbb{X}^+ = [\mathbf{x}(t_2) \mid \cdots \mid \mathbf{x}(t_{N_t})] \in \mathbb{R}^{N_h \times (N_t-1)}$;
Compute the Singular Value Decomposition (SVD):
$\mathbb{X}^- = \mathbb{U}_M \Sigma_M \mathbb{V}_M^*$;
Compute best fit operator: $\mathbb{A} = \mathbb{X}^+ \mathbb{V}_M \Sigma_M^{-1} \mathbb{U}_M^* \in \mathbb{R}^{N_h \times N_h}$;
Project $\mathbb{A}$ onto the modes with rank M:
$\tilde{\mathbb{A}} = \mathbb{U}_M^* \mathbb{A} \mathbb{U}_M \in \mathbb{R}^{M \times M}$

Appendix. DMD algorithm

In this appendix a scheme of the logic underlying the DMD procedure is reported.

Data availability

Data will be made available on request.

References

[1] J.P. Freidberg, Ideal MHD, Cambridge University Press, 2014.
[2] H. Zohm, G. Gantenbein, A. Isayama, A. Keller, R. La Haye, M. Maraschek, A. Mück, K. Nagasaki, S. Pinches, E. Strait, MHD limits to tokamak operation and their control, Plasma Phys. Control. Fusion 45 (12A) (2003) A163.
[3] S. Molokov, R. Moreau, K. Moffatt, L. Bühler, Liquid metal magnetohydrodynamics for fusion blankets, Magnetohydrodyn.: Hist. Evol. Trends (2007) 171–194.
[4] G. Ferrero, R. Testoni, M. Zucchetti, Impact assessment of radiative heat transport in ARC-class reactor flibe liquid immersion blanket, Nucl. Sci. Eng. (2023) 1–16.
[5] D. Biskamp, Nonlinear Magnetohydrodynamics, first ed., Cambridge University Press, 1997.
[6] M. Lo Verso, C. Introini, L. Barucca, M. Caramello, M. Di Prinzio, F. Giacobbo, L. Savoldi, A. Cammi, Non-modal stability analysis of magneto-hydrodynamic flow in a single pipe, Fundam. Plasma Phys. 10 (2024) 100042.
[7] T. Lassila, A. Manzoni, A. Quarteroni, G. Rozza, Model order reduction in fluid dynamics: challenges and perspectives, Reduc. Order Methods Model. Comput. Reduct. (2014) 235–273.
[8] G. Rozza, M. Hess, G. Stabile, M. Tezzele, F. Ballarin, C. Gräßle, M. Hinze, S. Volkwein, F. Chinesta, P. Ladeveze, Y. Maday, A. Patera, J. Farhat Char, Model Order Reduction: Volume 2: Snapshot-Based Methods and Algorithms, De Gruyter, 2020.
[9] A. Quarteroni, A. Manzoni, F. Negri, Reduced Basis Methods for Partial Differential Equations: An Introduction, first ed., in: UNITEXT, Springer Cham, 2015.
[10] S. Lorenzi, A. Cammi, L. Luzzi, G. Rozza, POD-Galerkin method for finite volume approximation of Navier–Stokes and RANS equations, Comput. Methods Appl. Mech. Engrg. 311 (2016) 151–179, Publisher: Elsevier B.V.
[11] M. Tezzele, N. Demo, A. Mola, G. Rozza, An integrated data-driven computational pipeline with model order reduction for industrial and applied mathematics, in: Novel Mathematics Inspired by Industrial Challenges, Springer, 2022, pp. 179–200.
[12] A. Charalampopoulos, T. Sapsis, Uncertainty quantification of turbulent systems via physically consistent and data-informed reduced-order models, Phys. Fluids 34 (7) (2022) 075120.
[13] A. Moni, W. Yao, H. Malekmohamadi, Data-driven reduced-order modeling for nonlinear aerodynamics using an autoencoder neural network, Phys. Fluids 36 (1) (2024) 016105.
[14] A. Sartori, A. Cammi, L. Luzzi, G. Rozza, A multi-physics reduced order model for the analysis of Lead Fast Reactor single channel, Ann. Nucl. Energy 87 (2016) 198–208.
[15] S. Lorenzi, A. Cammi, L. Luzzi, G. Rozza, A reduced order model for investigating the dynamics of the Gen-IV LFR coolant pool, Appl. Math. Model. 46 (2017) 263–284.
[16] R. Taylor, J.N. Kutz, K. Morgan, B.A. Nelson, Dynamic mode decomposition for plasma diagnostics and validation, Rev. Sci. Instrum. 89 (5) (2018) 053501.

[17] A.A. Kaptanoglu, K.D. Morgan, C.J. Hansen, S.L. Brunton, Physics-constrained, low-dimensional models for magnetohydrodynamics: First-principles and data-driven approaches, Phys. Rev. E 104 (1) (2021) 015206.
[18] S.L. Brunton, J.L. Proctor, J.N. Kutz, Discovering governing equations from data by sparse identification of nonlinear dynamical systems, Proc. Natl. Acad. Sci. USA 113 (15) (2016) 3932–3937.
[19] A.A. Kaptanoglu, K.D. Morgan, C.J. Hansen, S.L. Brunton, Characterizing magnetized plasmas with dynamic mode decomposition, Phys. Plasmas 27 (3) (2020).
[20] M. Lo Verso, S. Riva, C. Introini, E. Cervi, F. Giacobbo, L. Savoldi, M. Di Prinzio, M. Caramello, L. Barucca, A. Cammi, Application of a non-intrusive reduced order modeling approach to magnetohydrodynamics, Phys. Fluids 36 (10) (2024).
[21] P.J. Schmid, Dynamic Mode Decomposition of numerical and experimental data, J. Fluid Mech. 656 (2010) 5–28, Publisher: Cambridge University Press.
[22] S.L. Brunton, J.N. Kutz, Data-Driven Science and Engineering: Machine Learning, Dynamical Systems, and Control, second ed., Cambridge University Press, USA, 2022.
[23] N. Demo, M. Tezzele, G. Rozza, PyDMD: Python Dynamic Mode Decomposition, J. Open Source Softw. 3 (22) (2018) 530, Publisher: The Open Journal.
[24] S.M. Ichinaga, F. Andreuzzi, N. Demo, M. Tezzele, K. Lapo, G. Rozza, S.L. Brunton, J.N. Kutz, PyDMD: A Python package for robust dynamic mode decomposition, 2024.
[25] T. Askham, J.N. Kutz, Variable projection methods for an optimized dynamic mode decomposition, SIAM J. Appl. Dyn. Syst. 17 (1) (2018) 380–416.
[26] J.H. Tu, C.W. Rowley, D.M. Luchtenburg, S.L. Brunton, J.N. Kutz, On dynamic mode decomposition: Theory and applications, J. Comput. Dyn. 1 (2) (2014) 391–421.
[27] U. Müller, L. Bühler, Magnetofluiddynamics in Channels and Containers, Springer Science & Business Media, 2001.
[28] M. Lo Verso, C. Introini, E. Cervi, F. Giacobbo, A. Cammi, A novel openfoam library for magneto-hydrodynamics studies in the nuclear fusion field, in: Proceedings of the NUTHOS-14 International Conference, August 25–28, 2024, Vancouver, CAN, 2024.
[29] M. Bachmayr, A. Cohen, Kolmogorov widths and low-rank approximations of parametric elliptic PDEs, Math. Comp. 86 (304) (2017) 701–724, http://dx.doi.org/10.1090/mcom/3132, URL https://www.ams.org/mcom/2017-86-304/S0025-5718-2016-03132-4/.
[30] D. Lee, H. Choi, Magnetohydrodynamic turbulent flow in a channel at low magnetic Reynolds number, J. Fluid Mech. 439 (2001) 367–394.